Inertia Effect in Two-Dimensional MHD Channel Flow under a Traveling Sine Wave Magnetic Field

doi: 10.1063/1.858125

Inertia effect in two-dimensional MHD channel flow under a traveling sine wave magnetic field

Kazuyuki Ueno
Department of Aeronautical Engineering, Kyoto University, Kyoto 606, Japan

(Received 12 March 1991; accepted 20 August 1991)

The inertia effect peculiar to the MHD flow under a traveling sine wave transverse magnetic field between two parallel walls is investigated analytically and numerically. Solutions for steady flow of incompressible viscous fluid are obtained on the coordinate system moving with the traveling magnetic field. The flow is classified by interaction parameter N into three categories. (i) In the case of $N \gg H_a^3$ (H_a: average Hartmann number), inertia effect is negligibly small and the local force balance in each cross section is the same as that in the Hartmann flow characterized by H_l (H_l: local Hartmann number which is spatially periodic). (ii) In the case of $1 \lesssim N \lesssim H_a^3$, appreciable inertia effect appears in the region where the local magnetic field is smaller than $N^{-1/3}B_0$ (B_0: the amplitude of sine wave magnetic field). (iii) In the case of $N \ll 1$, a new type boundary layer appears, where the periodic part of the Lorentz force is balanced by inertia force. The inertia effect to the power output and the efficiency of an MHD induction generator is very small in spite of the remarkable change in the flow field.

I. INTRODUCTION

Magnetohydrodynamic (MHD) flow under a traveling alternating magnetic field, associated with a liquid metal induction generator,[1-3] has been investigated since the 1960s. Most of the analytical investigations concentrated on topics of winding loss and end loss. In such analyses, they neglected the viscosity of fluid and assumed a uniform velocity throughout the channel. Wang and Dudzinsky,[2] comparing their experimental result with such an analysis, suggested that low efficiency in the experiment may be attributed to the high friction loss. In a previous paper,[4] we analyzed the two-dimensional flow field for $N \sim 1$ considering fluid friction, where N is interaction parameter. But it was shown that friction loss is small order of H_a^{-1} compared with power input, where H_a is average Hartmann number and it is much larger than unity in a MHD induction generator in general. In order to explain the loss observed on the experiment, further investigation is needed. On the other hand, recently, much attention is paid to the flow field for $N \gg 1$ associated with MHD metallurgy.[5]

In this paper we proceed with the investigation, comparing the flow under a traveling sine wave magnetic field with Hartmann flow[6,7] which is a MHD flow under a uniform magnetic field between two parallel walls. The flow in our problem will have a more complicated structure than Hartmann flow for the following three possible reasons.

(i) Inertia has a contribution to the flow field, since the flow cannot be parallel flow by reason of the existence of a spatially periodic Lorentz force.

(ii) The imposed magnetic field becomes weaker with distance from the wall and it not only has the transverse component but also the parallel component to the wall.

(iii) The deformation of magnetic field (which is induced by the current in channel) has a contribution not only to the pressure but also to the velocity. Then, the interaction between flow field and magnetic field is more complicated.

Investigation of the effects of (i)–(iii) will give us a fundamental knowledge of MHD flow in the presence of an alternating magnetic field.

In order to classify this problem, we introduce five nondimensional parameters H_a, N, K, Λ, and G. Parameters N, Λ, and K correspond to (i), (ii) and (iii), above, respectively. The main purpose of this paper is to make clear the effect of (i). In order to simplify the problem, we assume $K \to 0$ and $\Lambda \to \infty$. Under these assumptions, the effects of (ii) and (iii) are negligibly small. We show the solutions of flow field for various N in the coordinate system moving with traveling magnetic field, where we can assume the flow field and the magnetic field are steady. These solutions make clear the local force balance in the flow field and the structure of boundary layer. We apply the results of analyses to a MHD induction generator. It gives us the relation between N, representing the effect of fluid inertia, and the characteristics of the generator.

II. GOVERNING EQUATIONS

A. Formulation of problem

In this section we first consider a three-dimensional problem in the coordinate system moving with the traveling magnetic field. Then, we discuss the possible two-dimensional problem under some reasonable assumptions, and formulate it.

Figure 1 shows the configuration of the flow field and the magnetic field in a straight rectangular duct. In the figure, $\mathbf{u}' = (u', v', w')$ denotes the flow velocity, $\mathbf{B}' = (B_x', B_y', B_z')$ the magnetic flux density, and λ the wavelength of the sine wave magnetic field. The walls at $y' = \pm h$ are assumed to be insulators and the walls at $z' = \pm b$ to be perfect conductors. The two conductor walls have been shown to be equipotential surfaces and of the same electric potential (see Appendix A or Ref. 4).

The boundary condition for the flow velocity is given by

$$u' = -U_s, \quad v' = 0, \quad w' = 0 \tag{1}$$

 0899-8213/91/123107-10$02.00

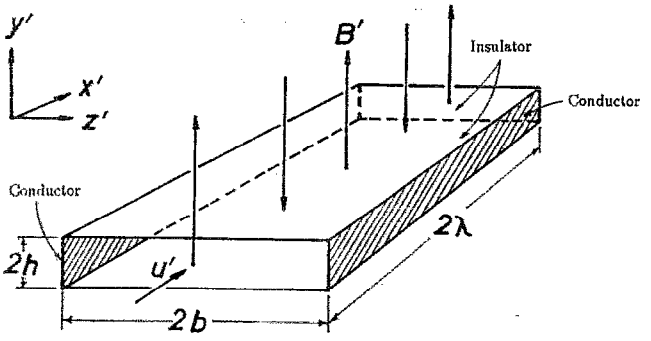

FIG. 1. Configuration of the flow and magnetic fields in a straight rectangular duct.

on the walls $y' = \pm h$ and $z' = \pm b$, where U_s denotes the phase velocity of the traveling magnetic field. As the boundary condition for the magnetic field, we assume

$$B'_y = B_0 \sin(2\pi x'/\lambda) \tag{2a}$$

on the walls $y' = \pm h$ and

$$B'_z = 0 \tag{2b}$$

on the walls $z' = \pm b$, even if the current in the duct distorts the magnetic field. From above boundary conditions, we can assume that $\mathbf{u}'$, $\mathbf{B}'$, the electric field $\mathbf{E}'$, and the current density $\mathbf{j}'$ are steady and periodic with respect to x'. The pressure gradient is also assumed to be steady and periodic, though the pressure p' contains an aperiodic part $-P_{x0}(x' + U_s t')$. Indeed this average pressure gradient $-P_{x0}$ drives the fluid in one direction.

In order to formulate the two-dimensional problem, we need to assume

$$w' = 0, \quad B'_z = 0, \quad E'_x = 0, \quad E'_y = 0, \tag{3a}$$

and all the variables are independent of z' in the flow region except for the boundary layers on the conductor walls. The conductor walls at $z' = \pm b$ are of the same electric potential (Appendix A) and E'_z is also assumed to be independent of z', then

$$E'_z = 0. \tag{3b}$$

For the case of uniform magnetic field, Hunt and Stewartson[8] showed that the boundary layers on the conductor walls do not affect the two-dimensional configuration in the other flow region if the Hartmann number and the aspect ratio b/h are large enough. But it is difficult to verify that the above situation is valid for the case of alternating magnetic field, since the boundary layers on the conductor walls have a three-dimensional structure.

Here, we assume that a two-dimensional flow field is possible for the sine wave magnetic field, and we consider a two-dimensional flow field between two parallel insulator walls as shown in Fig. 2. Then, the governing equations can be written as follows:

$$\frac{\partial u'}{\partial x'} + \frac{\partial v'}{\partial y'} = 0, \tag{4a}$$

$$\rho_L\left(u'\frac{\partial u'}{\partial x'} + v'\frac{\partial u'}{\partial y'}\right) = -\frac{\partial p'}{\partial x'} + \eta_L\left(\frac{\partial^2 u'}{\partial x'^2} + \frac{\partial^2 u'}{\partial y'^2}\right) - j'_z B'_y, \tag{4b}$$

$$\rho_L\left(u'\frac{\partial v'}{\partial x'} + v'\frac{\partial v'}{\partial y'}\right) = -\frac{\partial p'}{\partial y'} + \eta_L\left(\frac{\partial^2 v'}{\partial x'^2} + \frac{\partial^2 v'}{\partial y'^2}\right) + j'_z B'_x, \tag{4c}$$

$$j'_z = \sigma_L(u'B'_y - v'B'_x), \tag{4d}$$

$$\frac{\partial B'_x}{\partial x'} + \frac{\partial B'_y}{\partial y'} = 0, \tag{4e}$$

$$\frac{\partial B'_y}{\partial x'} - \frac{\partial B'_x}{\partial y'} = \mu_L j'_z, \tag{4f}$$

where ρ_L, η_L, σ_L, and μ_L are the density, viscosity, electric conductivity, and magnetic permeability of the fluid, respectively, all of which are assumed to be constants.

The analysis is simplified by using the scalar and vector potentials ϕ' and $\mathbf{A}' = (0,0,A'_z)$ defined as

$$\mathbf{B}' = \nabla'\phi' + \nabla' \times \mathbf{A}', \tag{5}$$

where $\nabla' = (\partial/\partial x', \partial/\partial y', 0)$. The potentials ϕ' and A'_z satisfy the boundary conditions

$$\frac{\partial \phi'}{\partial y'} = B_0 \sin\left(\frac{2\pi x'}{\lambda}\right), \quad A'_z = 0, \tag{6}$$

on the walls $y' = \pm h$. The first term on the right-hand side of Eq. (5) shows the irrotational magnetic field imposed externally and the second term shows the rotational magnetic field induced by the internal current. Substituting Eq. (5) into Eqs. (4e) and (4f), we obtain

$$\frac{\partial^2 \phi'}{\partial x'^2} + \frac{\partial^2 \phi'}{\partial y'^2} = 0, \tag{7a}$$

$$\frac{\partial^2 A'_z}{\partial x'^2} + \frac{\partial^2 A'_z}{\partial y'^2} = -\sigma_L \mu_L\left[u'\left(\frac{\partial \phi'}{\partial y'} - \frac{\partial A'_z}{\partial x'}\right) - v'\left(\frac{\partial \phi'}{\partial x'} + \frac{\partial A'_z}{\partial y'}\right)\right], \tag{7b}$$

where we use the relation of Eq. (4d).

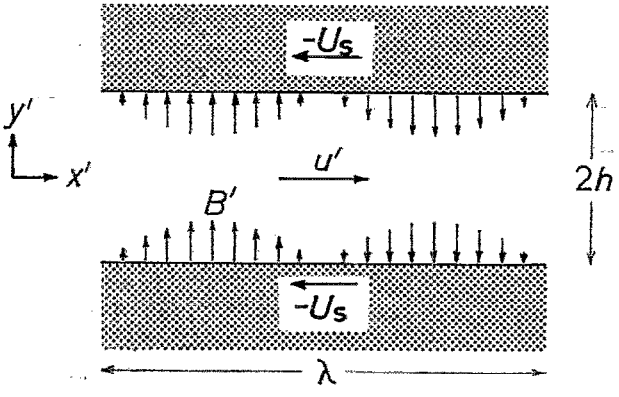

FIG. 2. Configuration of two-dimensional flow and magnetic fields between two parallel insulator walls.

B. Normalization

This problem has two characteristic lengths $\lambda/2\pi$ and h, which are independent of each other. On choosing the nondimensional parameters, we use $\lambda/2\pi$ or h so that the parameters can appropriately correspond to the construction of the flow and the magnetic fields.

The fluid is driven on the fundamental force balance between the pressure gradient and the Lorentz force. Then we can take the characteristic velocity as

$$U_0 \equiv \frac{P_{x0}}{\sigma_L (B_0/\sqrt{2})^2} = \frac{2P_{x0}}{\sigma_L B_0^2}. \tag{8}$$

We can estimate the viscous force at

$$\frac{1}{H_a^2} \equiv \frac{\eta_L U_0/h^2}{\sigma_L U_0 (B_0/\sqrt{2})^2} = \frac{2\eta_L}{\sigma_L h^2 B_0^2}, \tag{9}$$

compared with the Lorentz force, and the inertia force at

$$\frac{1}{N} \equiv \frac{\rho_L U_0^2/(\lambda/2\pi)}{\sigma_L U_0 (B_0/\sqrt{2})^2} = \frac{4\pi\rho_L U_0}{\sigma_L \lambda B_0^2} \tag{10}$$

compared with the Lorentz force. The nondimensional parameters H_a and N are referred to as average Hartmann number and interaction parameter, respectively.

The major contributive terms in Ampère's law, Eq. (7b), are $\partial^2 A_z'/\partial y'^2$ and $\sigma_L \mu_L u' \partial\phi'/\partial y'$. Then we can take the characteristic value of A_z' as

$$A_0 \equiv \sigma_L \mu_L h^2 U_0 B_0. \tag{11}$$

We can estimate the y' component of the induced magnetic field at

$$K \equiv \frac{A_0/(\lambda/2\pi)}{B_0} = \frac{2\pi\sigma_L\mu_L h^2 U_0}{\lambda} \tag{12}$$

compared with the y' component of the imposed magnetic field, and the x' component of the imposed magnetic field at

$$\frac{1}{\Lambda} \equiv \frac{hB_0/(\lambda/2\pi)}{B_0} = \frac{2\pi h}{\lambda} \tag{13}$$

compared with the y' component of the imposed magnetic field.

A set of five nondimensional parameters H_a, N, K, Λ, and

$$G \equiv U_s/U_0 \tag{14}$$

specifies a unique dynamically similar solution of the flow field and the magnetic field.

Now we write the problem in normalized nondimensional variables:

$$\begin{aligned} &x' = (\lambda/2\pi)x, \quad y' = hy, \\ &u' = U_0 u, \quad v' = (2\pi h/\lambda) U_0 v, \quad p' = (P_{x0}\lambda/2\pi)p, \\ &\phi' = hB_0\phi, \quad A_z' = A_0 A_z. \end{aligned} \tag{15}$$

Eliminating j_z' from Eqs. (4b) and (4c) by using Eq. (4d), and substituting Eq. (15) into Eqs. (4a)–(4c), (7a), and (7b), we obtain the following equations:

$$\frac{\partial u}{\partial x} + \frac{\partial v}{\partial y} = 0, \tag{16a}$$

$$\begin{aligned} \frac{1}{N}\left(u\frac{\partial u}{\partial x} + v\frac{\partial u}{\partial y}\right) = &-\frac{\partial p}{\partial x} + \frac{1}{H_a^2}\left(\frac{1}{\Lambda^2}\frac{\partial^2 u}{\partial x^2} + \frac{\partial^2 u}{\partial y^2}\right) \\ &- 2\left[u\left(\frac{\partial\phi}{\partial y} - K\frac{\partial A_z}{\partial x}\right)\right. \\ &\left. - v\left(\frac{1}{\Lambda^2}\frac{\partial\phi}{\partial x} + K\frac{\partial A_z}{\partial y}\right)\right] \\ &\times\left(\frac{\partial\phi}{\partial y} - K\frac{\partial A_z}{\partial x}\right), \end{aligned} \tag{16b}$$

$$\begin{aligned} \frac{1}{N\Lambda^2}\left(u\frac{\partial v}{\partial x} + v\frac{\partial v}{\partial y}\right) = &-\frac{\partial p}{\partial y} + \frac{1}{H_a^2\Lambda^2}\left(\frac{1}{\Lambda^2}\frac{\partial^2 v}{\partial x^2} + \frac{\partial^2 v}{\partial y^2}\right) \\ &+ 2\left[u\left(\frac{\partial\phi}{\partial y} - K\frac{\partial A_z}{\partial x}\right)\right. \\ &\left. - v\left(\frac{1}{\Lambda^2}\frac{\partial\phi}{\partial x} + K\frac{\partial A_z}{\partial y}\right)\right] \\ &\times\left(\frac{1}{\Lambda^2}\frac{\partial\phi}{\partial x} + K\frac{\partial A_z}{\partial y}\right), \end{aligned} \tag{16c}$$

$$\frac{1}{\Lambda^2}\frac{\partial^2\phi}{\partial x^2} + \frac{\partial^2\phi}{\partial y^2} = 0, \tag{16d}$$

$$\begin{aligned} \frac{1}{\Lambda^2}\frac{\partial^2 A_z}{\partial x^2} + \frac{\partial^2 A_z}{\partial y^2} = &-\left[u\left(\frac{\partial\phi}{\partial y} - K\frac{\partial A_z}{\partial x}\right)\right. \\ &\left. - v\left(\frac{1}{\Lambda^2}\frac{\partial\phi}{\partial x} + K\frac{\partial A_z}{\partial y}\right)\right]. \end{aligned} \tag{16e}$$

The boundary conditions are represented as

$$u = -G, \quad v = 0, \tag{17a}$$

$$\frac{\partial\phi}{\partial y} = \sin x, \quad A_z = 0, \tag{17b}$$

on the walls $y = \pm 1$. The average pressure gradient is -1 in the nondimensional form. Each nondimensional variable is expected to be the order of unity.

III. ANALYSIS AND DISCUSSION

In this section, we make clear the relation between the structure of the flow field and the interaction parameter N, which represents the effect of fluid inertia. In order to simplify the problem, we assume

$$K \to 0 \quad \text{and} \quad \Lambda \to \infty. \tag{18}$$

Under these assumptions, Eq. (16d) reduces to $\partial^2\phi/\partial y^2 = 0$, and the solution can be easily found:

$$\phi = y \sin x. \tag{19}$$

Substituting Eqs. (18) and (19) into Eqs. (16), we obtain

$$\frac{\partial u}{\partial x} + \frac{\partial v}{\partial y} = 0, \tag{20a}$$

$$\begin{aligned} &\frac{1}{N}\left(u\frac{\partial u}{\partial x} + v\frac{\partial u}{\partial y}\right) \\ &\quad = -\frac{\partial p}{\partial x} + \frac{1}{H_a^2}\frac{\partial^2 u}{\partial y^2} - u(1 - \cos 2x), \end{aligned} \tag{20b}$$

$$0 = -\frac{\partial p}{\partial y}, \tag{20c}$$

$$\frac{\partial^2 A_z}{\partial y^2} = -u \sin x. \tag{20d}$$

Equations (19) and (20b)–(20d) have the following three features, which come from the assumptions of Eqs. (18). (i) The y component of the imposed magnetic field is constant across the channel. (ii) The x component of imposed magnetic field has no contribution to the flow field. (iii) The induced magnetic field is determined by Eq. (20d), but it has no contribution to the flow field.

A. Analytical solution for a large interaction parameter

In this subsection, we analyze the case of

$$N \to \infty \tag{21}$$

analytically. The analysis is simplified by using the streamfunction $\psi(x,y)$ defined as

$$u = \frac{\partial \psi}{\partial y}, \quad v = -\frac{\partial \psi}{\partial x}. \tag{22}$$

The continuity equation (20a) is satisfied automatically by using the streamfunction. We define the local Hartmann number as

$$H_l(x) \equiv \sqrt{2} H_a \sin x. \tag{23}$$

Differentiating the momentum equation (20b) with y, we have

$$\frac{\partial^4 \psi}{\partial y^4} - H_l^2 \frac{\partial^2 \psi}{\partial y^2} = 0,$$

where we have taken account of Eqs. (20c) and (21)–(23). Rewriting the boundary conditions (17a) by using the streamfunction, we have

$$\frac{\partial \psi}{\partial y} = -G, \quad \psi = \pm \Psi_w,$$

at $y = \pm 1$, where the constant Ψ_w denotes a half of the nondimensional flow rate. We can find the solution as

$$\psi = \Psi_w y - (\Psi_w + G) \frac{\sinh H_l y - y \sinh H_l}{H_l \cosh H_l - \sinh H_l}. \tag{24}$$

Substituting Eq. (24) into the first equation of (22), we obtain

$$u = \Psi_w - (\Psi_w + G) \frac{H_l \cosh H_l y - \sinh H_l}{H_l \cosh H_l - \sinh H_l}. \tag{25}$$

In order to determine Ψ_w, we integrate the momentum equation (20b) from $x = -\pi$ to $x = \pi$ and from $y = -1$ to $y = 1$. Considering that the average pressure gradient is -1, Eq. (20b) reduces to

$$0 = 1 + \frac{1}{2\pi H_a^2} \int_{-\pi}^{\pi} \left(\frac{\partial u}{\partial y} \right)_{y=1} dx - \Psi_w.$$

Substituting Eq. (25) into this equation, we obtain

$$\Psi_w = 1 - (1 + G) \frac{\int_{-\pi}^{\pi} [H_l^2 \sinh H_l / (H_l \cosh H_l - \sinh H_l)] dx}{2\pi H_a^2 + \int_{-\pi}^{\pi} [H_l^2 \sinh H_l / (H_l \cosh H_l - \sinh H_l)] dx}. \tag{26}$$

The integration in the right-hand side has to be carried out numerically.

Figure 3 shows typical distributions of the velocity u in various cross sections over one wavelength of the channel. The local force balance in the flow field is the same as that of Hartmann flow, though the boundary layer in each cross section is characterized by $H_l(x)$ rather than H_a. Therefore, the thickness of the boundary layer varies periodically with x. In the region of $|H_l(x)| \lesssim 1$, the boundary layer extends over the channel cross section. Particularly, Poiseuille distribution appears in the cross section at $x = m\pi$ (m is integer), where $H_l = 0$.

B. Numerical solutions for various interaction parameters

In this subsection, we find the steady solutions numerically as converged solutions of the corresponding initial value problems for various N. In order to solve the initial value problem, we use the Marker-and-Cell (MAC) method[9] which is improved for the case of $\Lambda \to \infty$ (see Appendix B).

If u^n is given at certain time $t = n\Delta t$, u^{n+1} at next time $t = (n+1)\Delta t$ can be obtained by the following procedure. First, the nondimensional flow rate Ψ_w^n is calculated by the relation

$$\Psi_w(x) = \int_0^1 u \, dy, \tag{27}$$

where we treat Ψ_w not as a constant but as a function of x. Second, the velocity v^n is determined by the relation

$$v = -\frac{\partial}{\partial x} \int_0^y u \, dy + \frac{\partial \Psi_w}{\partial x} y. \tag{28}$$

Third, we solve

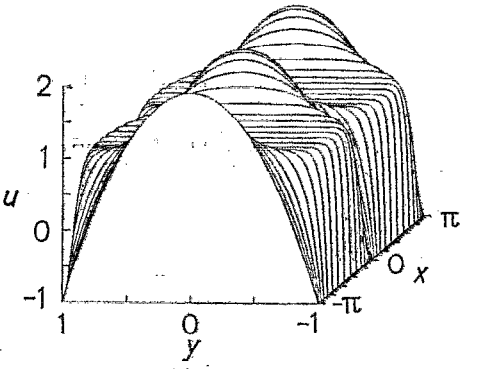

FIG. 3. Distributions of u in various cross sections of the analytical solution for $N \to \infty$, $H_a = 31.6$, and $G = 1$.

$$\frac{\partial^2 p}{\partial x^2} = -\frac{1}{N}\frac{\partial}{\partial x}\int_0^1 \left(u\frac{\partial u}{\partial x} + v\frac{\partial u}{\partial y}\right) dy + \frac{1}{H_a^2}\left(\frac{\partial^2 u}{\partial x\,\partial y}\right)_{y=1} - \frac{\partial}{\partial x}\left[\Psi_w(1-\cos 2x)\right] + \frac{1}{\Delta t}\frac{\partial \Psi_w}{\partial x}, \tag{29}$$

to obtain p^n, substituting u^n, v^n, and Ψ_w^n into the right-hand side. Although $\partial\Psi_w/\partial x$ is identically zero due to the continuity equation, it is retained in Eqs. (28) and (29) as a correction term in order to prevent the accumulation of numerical errors. Fourth, the momentum equation

$$\frac{\partial u}{\partial t} + \frac{1}{N}\left(u\frac{\partial u}{\partial x} + v\frac{\partial u}{\partial y}\right) = -\frac{\partial p}{\partial x} + \frac{1}{H_a^2}\frac{\partial^2 u}{\partial y^2} - u(1-\cos 2x) \tag{30}$$

is integrated with t to obtain u^{n+1} [the time t' has been normalized by the relation of $t' = (2\rho_L/\sigma_L B_0^2)t$].

On the above procedure, we require the boundary conditions

$$\begin{aligned} &\frac{\partial u}{\partial y} = 0, \quad v = 0, \quad \text{at } y = 0, \\ &u = -G, \quad v = 0, \quad \text{at } y = 1, \\ &u(x+\pi, y) = u(x,y), \quad v(x+\pi, y) = v(x,y), \\ &p(x+\pi) = p(x) - \pi, \end{aligned} \tag{31}$$

considering the symmetry and the periodicity.

We use the Euler backward scheme

$$\frac{u^{n+1}-u^n}{\Delta t} + \frac{1}{N}\left(u^n\frac{\partial u^{n+1}}{\partial x} + v^n\frac{\partial u^{n+1}}{\partial y}\right) = -\frac{\partial p^n}{\partial x} + \frac{1}{H_a^2}\frac{\partial^2 u^{n+1}}{\partial y^2} - u^{n+1}(1-\cos 2x) \tag{32}$$

to integrate Eq. (30), where the second term of the left-hand side is linearized as

$$\frac{1}{N}\left(u^{n+1}\frac{\partial u^{n+1}}{\partial x} + v^{n+1}\frac{\partial u^{n+1}}{\partial y}\right) \approx \frac{1}{N}\left(u^n\frac{\partial u^{n+1}}{\partial x} + v^n\frac{\partial u^{n+1}}{\partial y}\right).$$

We employ the 100×50 irregular rectangular staggered mesh system to evaluate u, v, and p at each mesh point (50 mesh points along the line of $x = \text{const}$ have the same value of p). All the spatial derivatives, except for the nonlinear terms, are approximated by the central difference. The nonlinear terms are approximated by the third-order upwind scheme by Kawamura and Kuwahara.[10] The finite-difference equations by discretizing Eqs. (29) and (32) are solved by the Gauss–Seidel method.

For our converged solutions, the error of the continuity equation $\partial\Psi_w/\partial x$ is smaller than 5.7×10^{-4}.

Figures 4(a)–4(d) show typical distributions of u in various cross sections over one wavelength of the channel (we show the region $-\pi \leqslant x \leqslant \pi$ and $-1 \leqslant y \leqslant 1$, though we

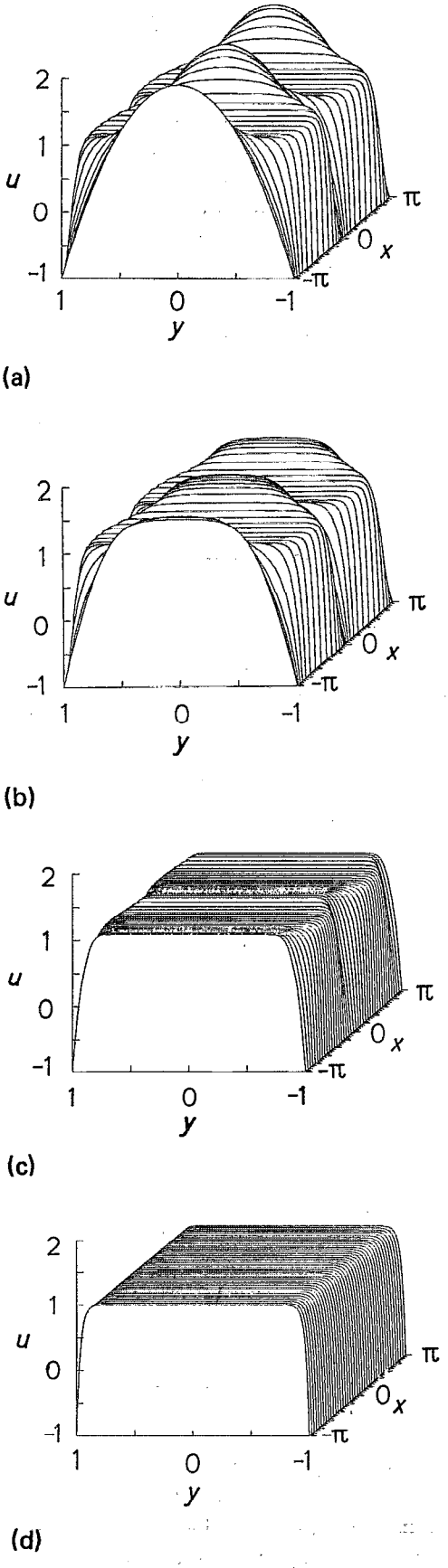

FIG. 4. Distributions of u in various cross sections of the numerical solutions. (a) $N = 5.03\times 10^3$, $H_a = 31.6$, $G = 1$; (b) $N = 1.59\times 10^2$, $H_a = 31.6$, $G = 1$; (c) $N = 1.59$, $H_a = 31.6$, $G = 1$; (d) $N = 1.59\times 10^{-2}$, $H_a = 31.6$, $G = 1$.

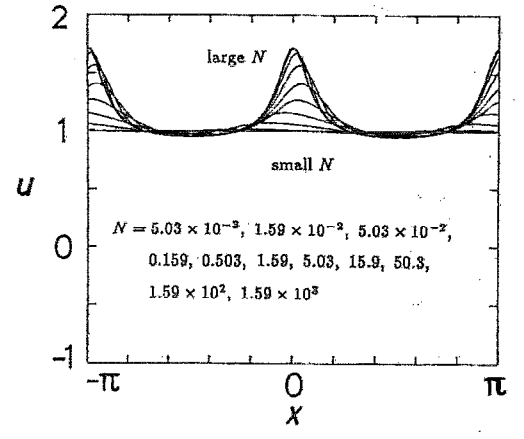

(a)

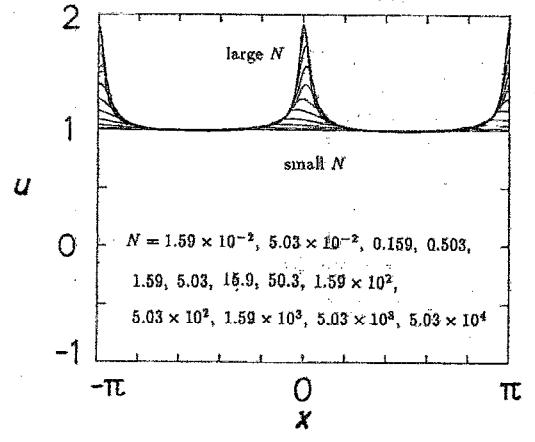

(b)

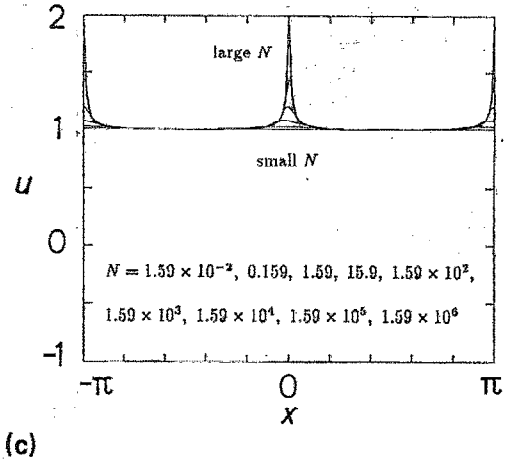

(c)

FIG. 5. Distributions of u on the central plane $y = 0$ for various N. (a) $H_a = 10$, $G = 1$; (b) $H_a = 31.6$, $G = 1$; (c) $H_a = 100$, $G = 1$.

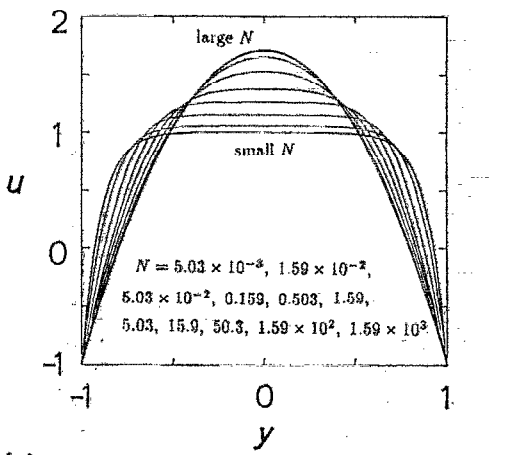

(a)

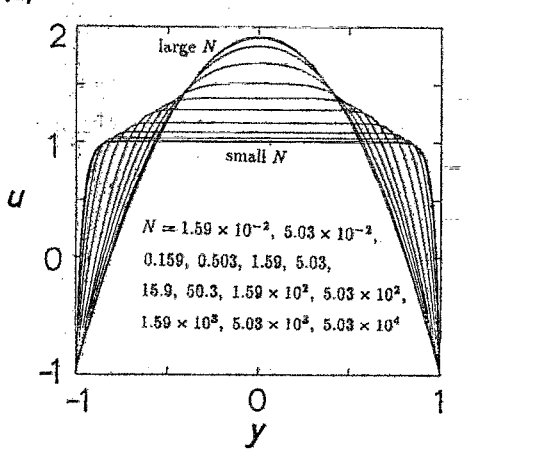

(b)

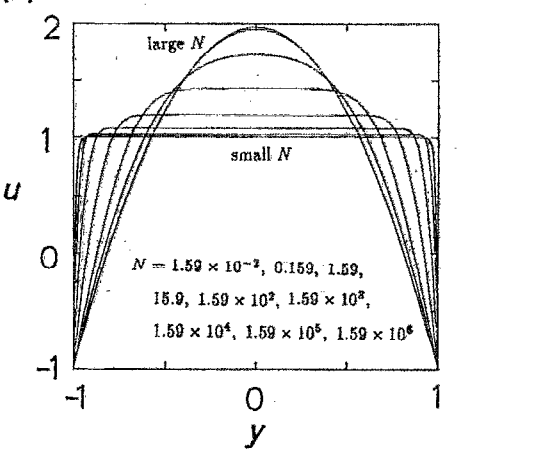

(c)

FIG. 6. Distributions of u in the cross section at $x = m\pi$ (m is integer) for various N. (a) $H_a = 10$, $G = 1$; (b) $H_a = 31.6$, $G = 1$; (c) $H_a = 100$, $G = 1$.

solve the region $0 \leqslant x \leqslant \pi$ and $0 \leqslant y \leqslant 1$). Figures 5(a)–5(c) show the distributions of u on the central plane $y = 0$ for various N. We can classify the solutions by N into three categories. (i) In the case of $N \gg H_a^3$, the inertia effect is negligibly small throughout the flow field, then the flow field approximately agrees with the flow which has been given analytically in the last subsection. (ii) In the case of $1 \lesssim N \lesssim H_a^3$, the inertia effect is remarkable in the region of $|\sin x| \lesssim N^{-1/3}$. (iii) In the case of $N \ll 1$, the velocity is similar to Hartmann flow.

Figures 6(a)–6(c) show the distributions of u in the cross section at $x = m\pi$ (m is an integer) for various N. When we define the thickness of the boundary layer as

$$\delta \equiv \int_0^1 \left(1 - \frac{G + u(m\pi, y)}{G + u(m\pi, 0)}\right) dy, \tag{33}$$

δ is obtained versus $H_a^{-1}N^{1/3}$ as in Fig. 7. For category (i), δ is approximately equal to 1/3, since the distribution of u agrees with Poiseuille flow in good approximation. For category (ii), inertia force has the same order as the Lorentz force in the region of $|\sin x| \lesssim N^{-1/3}$. Then, the ratio of the inertia force to the viscous force in this region, that is to say, local Reynolds number is $H_a^2 N^{-2/3}$, and δ is the order of $H_a^{-1}N^{1/3}$. For category (iii), δ is approximately equal to $1/H_a$, since the distribution of u is similar to Hartmann flow.

C. Force balance for small interaction parameter

The numerical solutions in the last subsection show that the velocity distribution for $N \ll 1$ is similar to that in Hartmann flow,

$$u = 1 - (1+G)\,(\cosh H_a y/\cosh H_a), \tag{34a}$$

$$v = 0, \tag{34b}$$

$$p = -x, \tag{34c}$$

which can be obtained if the term of $\cos 2x$ is dropped from Eq. (20b). Here, we try to obtain the solutions for

$$N \ll 1, \quad H_a \gg 1, \quad G \sim 1, \tag{35}$$

by adding some correction terms to Eqs. (34) and make clear the local force balance in the flow field and the structure of boundary layers under the assumption of laminar flow (see Appendix C: stability of the flow for small N).

1. Core flow

In the core region, the second term on the right-hand side of Eq. (34a) is negligibly small. Substituting $u = 1$ into Eq. (20b), we find a periodic variation term

$$\cos 2x \tag{36}$$

in the Lorentz force terms. This is a peculiar term for the sine wave magnetic field. This force can be balanced by the pressure gradient alone. Then, by adding the correction term to Eq. (34c), the pressure is obtained as

$$p = -x + \tfrac{1}{2}\sin 2x. \tag{37}$$

2. Boundary layer

We consider the boundary layer on the wall at $y = 1$. We introduce the stretched coordinate

$$\eta = H_a(1-y) \tag{38}$$

to analyze the flow field in the boundary layer. Then, Eqs. (20a)–(20c) reduce to

$$\frac{\partial u}{\partial x} - H_a \frac{\partial v}{\partial \eta} = 0, \tag{39a}$$

$$\frac{1}{N}\left(u\frac{\partial u}{\partial x} - H_a v\frac{\partial u}{\partial \eta}\right) = -\frac{\partial p}{\partial x} + \frac{\partial^2 u}{\partial \eta^2} - u(1-\cos 2x), \tag{39b}$$

$$0 = \frac{\partial p}{\partial \eta}. \tag{39c}$$

In this layer, Eq. (34a) approximate to $u = 1 - (1+G)\exp(-\eta)$. Substituting this into Eq. (39b), we can find a term

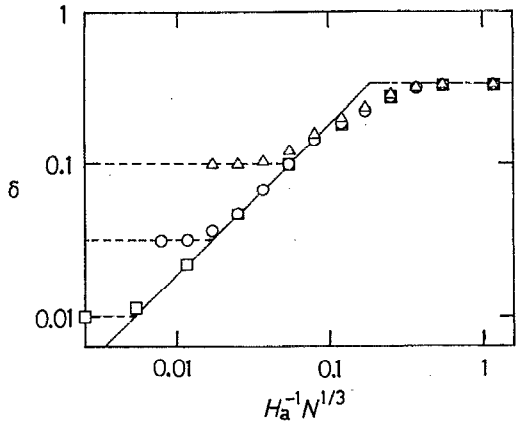

FIG. 7. The thickness of boundary layer δ. △, the numerical solutions for $H_a = 10$, $G = 1$; ○, the numerical solutions for $H_a = 31.6$, $G = 1$; □, the numerical solutions for $H_a = 100$, $G = 1$; – – –, Poiseuille flow; ----, Hartmann flow for $H_a = 10$, 31.6, and 100.

$$[1 - (1+G)\exp(-\eta)]\cos 2x \tag{40}$$

in the Lorentz force terms. This is a peculiar term for the sine wave magnetic field.

The force shown by the first term in brackets of Eq. (40) is the same as the force shown by Eq. (36); it can then be balanced by the pressure gradient. On the other hand, the force shown by the second term in brackets causes the alternation of velocity. We assume the solutions for the velocity in the form

$$u = 1 - (1+G)\exp(-\eta) + N u_a(x,\eta), \tag{41a}$$

$$v = H_a^{-1} N v_a(x,\eta), \tag{41b}$$

where u_a and v_a are unit order periodic functions that satisfy $\int_0^1 u_a\,dx = 0$ and $\int_0^1 v_a\,dx = 0$. Substituting Eqs. (37) and (41) into Eqs. (39), and neglecting small-order terms, we obtain

$$\frac{\partial u_a}{\partial x} - \frac{\partial v_a}{\partial \eta} = 0, \tag{42a}$$

$$[1 - (1+G)\exp(-\eta)]\frac{\partial u_a}{\partial x} - (1+G)\exp(-\eta)v_a = -(1+G)\exp(-\eta)\cos 2x. \tag{42b}$$

If we require a boundary condition

$$v_a = 0 \tag{43}$$

on the wall $\eta = 0$, the solutions are obtained as

$$u_a(x,\eta) = [(1+G)/2G]\exp(-\eta)\sin 2x, \tag{44a}$$

$$v_a(x,\eta) = [(1+G)/G][1 - \exp(-\eta)]\cos 2x. \tag{44b}$$

Both the second term of Eq. (41a) and u_a contain the factor $\exp[-H_a(1-y)]$, that is to say, the boundary layer has a thickness of the order H_a^{-1}. The former is formed on the balance between viscous force and the component of Lorentz force independent of x. On the other hand, the latter is formed on the balance between inertia force and the periodic

component of Lorentz force. The latter type of boundary layer is peculiar to the alternating magnetic field.

3. Sublayer

Equations (42) do not have enough degrees of freedom to satisfy all the boundary conditions. In fact, u_a does not vanish on the wall. This fact suggests the existence of a sublayer adjacent to the wall. Then, we stretch the coordinate further:

$$\zeta = N^{-1/2}\eta = H_a N^{-1/2}(1-y). \tag{45}$$

Equations (20a)–(20c) reduce to

$$\frac{\partial u}{\partial x} - \frac{H_a}{N^{1/2}}\frac{\partial v}{\partial \zeta} = 0, \tag{46a}$$

$$\frac{1}{N}\left(u\frac{\partial u}{\partial x} - \frac{H_a}{N^{1/2}}v\frac{\partial u}{\partial \zeta}\right) = -\frac{\partial p}{\partial x} + \frac{1}{N}\frac{\partial^2 u}{\partial \zeta^2} - u(1-\cos 2x), \tag{46b}$$

$$0 = \frac{\partial p}{\partial \zeta}. \tag{46c}$$

We assume the solutions for this sublayer in the form

$$u = -G + N^{1/2}(1+G)\zeta + N\left(-(1+G)\frac{\zeta^2}{2} + \frac{1+G}{2G}\sin 2x + u_b(x,\zeta)\right) + \cdots, \tag{47a}$$

$$v = H_a^{-1}N^{3/2}\left(\frac{1+G}{G}\zeta\cos 2x + v_b(x,\zeta)\right) + \cdots, \tag{47b}$$

where the terms containing u_b or v_b are the correction terms for the sublayer and the other terms are the Taylor expansion of Eqs. (41). Here, u_b and v_b are assumed to be unit order periodic functions, and u_b must tend to zero as $\zeta \to \infty$. Substituting Eqs. (37) and (47) into Eqs. (46), and neglecting small-order terms, we obtain

$$\frac{\partial u_b}{\partial x} - \frac{\partial v_b}{\partial \zeta} = 0, \tag{48a}$$

$$-G\frac{\partial u_b}{\partial x} = \frac{\partial^2 u_b}{\partial \zeta^2}. \tag{48b}$$

The boundary conditions are represented as

$$[(1+G)/2G]\sin 2x + u_b = 0, \tag{49a}$$

$$v_b = 0, \tag{49b}$$

on the wall $\zeta = 0$. The correction u_b is caused by u_a through the condition (49a), and formed on the balance between inertia force and viscous force.

The forms of Eqs. (48b) and (49a) agree with the momentum equation and the boundary condition for the flow field on an oscillating plane wall, though the inertia term of the momentum equation is time derivative for that problem.[11] This fact means that u_b is similar to the boundary layer on an oscillating plane wall dynamically.

The solutions for $G > 0$ are found as

$$u_b(x,\zeta) = [-(1+G)/2G]\exp(-G^{1/2}\zeta) \times \sin(2x + G^{1/2}\zeta), \tag{50a}$$

$$v_b(x,\zeta) = [(1+G)/2G^{3/2}][\sin 2x - \exp(-G^{1/2}\zeta) \times \sin(2x + G^{1/2}\zeta) - \cos 2x + \exp(-G^{1/2}\zeta) \times \cos(2x + G^{1/2}\zeta)]. \tag{50b}$$

The thickness of the sublayer is the order of $H_a^{-1}N^{1/2}$. If higher-order approximations of u, v, and p are desired, the above procedure can be extended according to the method of composite asymptotic expansion.[12]

IV. APPLICATION TO AN INDUCTION GENERATOR

The results of analysis in the channel are applied to an MHD induction generator that has an idealized stator shown in Fig. 8. The insulator wall is assumed to be thin enough and the winding of the stator is idealized into a current sheet, which has infinite conductivity in the z' direction but no current in the x' direction. The electromagnet iron placed outside above the current sheet is assumed to have infinite magnetic permeability and no current.

We take a closed circuit shown in Fig. 8. Since the wall and the current sheet are thin enough and the permeability of the electromagnet iron is infinity, Ampère's law is reduced to

$$\oint \frac{\mathbf{B}'}{\mu}\cdot d\mathbf{s}' = \left(\int \frac{B'_x}{\mu_L}dx'\right)_{y'=h-0} = \int J'_{cs}dx',$$

where J'_{cs} is the z' component of the sheet current density in the current sheet. Since we can take the closed circuit arbitrarily, we obtain

$$J'_{cs} = \frac{(B'_x)_{y'=h-0}}{\mu_L} = \frac{1}{\mu_L}\left(\frac{\partial \phi'}{\partial x'} + \frac{\partial A'_z}{\partial y'}\right)_{y'=h-0}. \tag{51}$$

In the current sheet, the relation

$$E'_{cs} = -(u'B'_y)_{y'=h} = U_s B_0 \sin(2\pi x'/\lambda), \tag{52}$$

must be satisfied according to Ohm's law, where E'_{cs} is the z' component of the electric field in the current sheet.

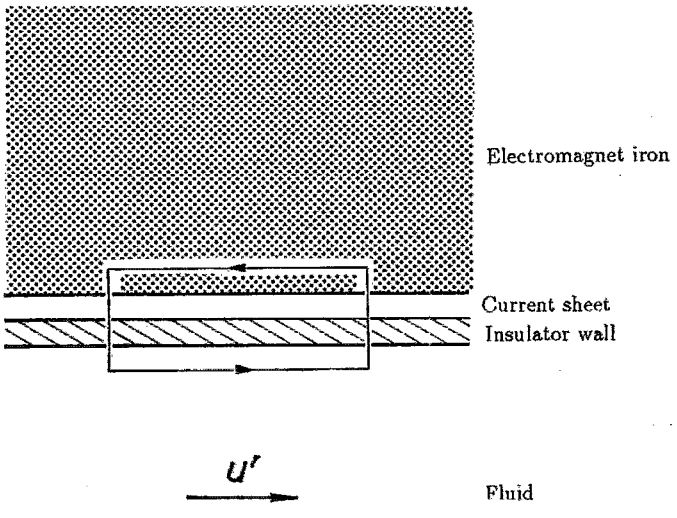

FIG. 8. Configuration of an idealized stator.

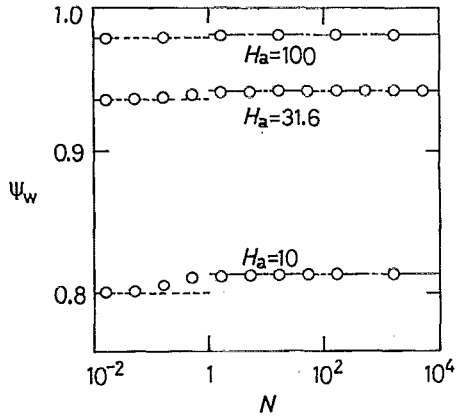

FIG. 9. A half of the nondimensional flow rate Ψ_w. O, the numerical solutions; - - -, the analytical solution for $N\to\infty$; ----, the analytical solution for $N\ll 1$.

The electrical power output per unit volume $P'_{\rm elec}$, the Ohmic loss per unit volume $P'_{\rm Ohm}$, the friction loss per unit volume $P'_{\rm fric}$, and the mechanical power input per unit volume $P'_{\rm mech}$ are given by

$$P'_{\rm elec}=\frac{1}{\lambda h}\int_0^{\lambda}(-J'_{cs}E'_{cs})dx',$$

$$P'_{\rm Ohm}=\frac{1}{\lambda h}\int_0^{h}\int_0^{\lambda}\frac{j'^2_z}{\sigma_L}dx'\,dy', \tag{53}$$

$$P'_{\rm fric}=\frac{1}{\lambda h}\int_0^{h}\int_0^{\lambda}2\eta_L\left[\left(\frac{\partial u'}{\partial x'}\right)^2+\frac{1}{2}\left(\frac{\partial v'}{\partial x'}+\frac{\partial u'}{\partial y'}\right)^2+\left(\frac{\partial v'}{\partial y'}\right)^2\right]dx'\,dy',$$

$$P'_{\rm mech}=\frac{1}{\lambda h}\int_0^{h}(u'+U_s)P_{x0}\lambda\,dy',$$

respectively. Using the above quantities, the conservation of energy is provided as

$$P'_{\rm mech}=P'_{\rm elec}+P'_{\rm Ohm}+P'_{\rm fric}. \tag{54}$$

When we can assume $\Lambda\to\infty$ and $K\to 0$, Eqs. (53) reduce to

$$P'_{\rm elec}=\sigma_L U_0^2(B_0/\sqrt{2})^2 G\Psi_w,$$

$$P'_{\rm Ohm}=\sigma_L U_0^2\left(\frac{B_0}{\sqrt{2}}\right)^2\frac{1}{\pi}\int_0^{1}\int_0^{\pi}u^2(1-\cos 2x)dx\,dy, \tag{55}$$

$$P'_{\rm fric}=\sigma_L U_0^2\left(\frac{B_0}{\sqrt{2}}\right)^2\frac{1}{\pi H_a^2}\int_0^{1}\int_0^{\pi}\left(\frac{\partial u}{\partial y}\right)^2dx\,dy,$$

$$P'_{\rm mech}=\sigma_L U_0^2\left(\frac{B_0}{\sqrt{2}}\right)^2(\Psi_w+G),$$

where we use the relations of Eqs. (15), (19), (20), (51), and (52). Though $P'_{\rm Ohm}$ and $P'_{\rm fric}$ are always positive, the signs of $P'_{\rm elec}$ and $P'_{\rm mech}$ can be changed with respect to G. The system works as a generator for $G>0$, while it works as a pump for $G<-\Psi_w$.

We can define the generator efficiency $\eta_{\rm eff}$ as

$$\eta_{\rm eff}\equiv P'_{\rm elec}/P'_{\rm mech}=\Psi_w G/(\Psi_w+G), \tag{56}$$

and the power factor F as

$$F^2\equiv\frac{\left[\int_0^{\lambda}(-J'_{cs}E'_{cs})dx'\right]^2}{\left(\int_0^{\lambda}J'^2_{cs}\,dx'\right)\left(\int_0^{\lambda}E'^2_{cs}\,dx'\right)}=\frac{K^2\Lambda^4\Psi_w^2}{1+K^2\Lambda^4\Psi_w^2}, \tag{57}$$

where the value of $K\Lambda^2$ has not been prescribed under the assumption $\Lambda\to\infty$ and $K\to 0$. The power factor F is required to be a large value in an actual induction generator, since the winding loss is greatly dependent on F.

The generator characteristics $P'_{\rm elec}$, $P'_{\rm mech}$, $\eta_{\rm eff}$, and F are expressed by simple relations with Ψ_w. Figure 9 shows Ψ_w vs N by using the results of Sec. III. The nondimensional flow rate Ψ_w slightly change with N, although the flow field remarkably changed with N. Then, we can conclude that the inertia effect to the generator characteristics is very small if Λ is sufficiently large and K is sufficiently small.

ACKNOWLEDGMENTS

The author gratefully acknowledges Professor Shigeki Morioka and Professor Ryuji Ishii for their helpful suggestions.

APPENDIX A: ELECTRIC POTENTIAL ON THE CONDUCTOR WALLS

The walls at $z'=\pm b$ are perfect conductors, therefore

$$\mathbf{E}'+\mathbf{u}'\times\mathbf{B}'=0$$

must be satisfied according to Ohm's law. Since $\mathbf{u}'=(-U_s,0,0)$ and $\mathbf{B}'=(B'_x,B'_y,0)$ on the walls, the parallel components of the electric field are

$$E'_x=0,\quad E'_y=0. \tag{A1}$$

Therefore, the inner surface of each conductor wall is an equipotential surface of the electric field.

We introduce a coordinate system shown by

$$x''=x'+\lambda/2,\quad y''=-y',\quad z''=-z'. \tag{A2}$$

Considering the symmetry and the periodicity with x', the velocity $\mathbf{u}''$ and the magnetic flux density $\mathbf{B}''$ on the $x''y''z''$ coordinate system are shown as

$$\mathbf{e}''_i\cdot\mathbf{u}''(x'',y'',z'')=\mathbf{e}'_i\cdot\mathbf{u}'(x',y',z'),$$
$$\mathbf{e}''_i\cdot\mathbf{B}''(x'',y'',z'')=\mathbf{e}'_i\cdot\mathbf{B}'(x',y',z'), \tag{A3}$$

where $\mathbf{e}'_i$ and $\mathbf{e}''_i$ are fundamental vectors. Therefore both the $x'y'z'$ and the $x''y''z''$ coordinate systems are equivalent. This fact suggests that we cannot distinguish the wall at $z'=b$ ($z''=-b$) from the wall at $z'=-b$ ($z''=b$). Then, both conductor walls must have the same electric potential.

APPENDIX B: IMPROVED MAC METHOD

For finite Λ and $K\to 0$, we have following equations according to the MAC method:

$$\frac{\partial u}{\partial t}+\frac{1}{N}\left(u\frac{\partial u}{\partial x}+v\frac{\partial u}{\partial y}\right)$$
$$=-\frac{\partial p}{\partial x}+\frac{1}{H_a^2}\left(\frac{1}{\Lambda^2}\frac{\partial^2 u}{\partial x^2}+\frac{\partial^2 u}{\partial y^2}\right)$$
$$-2\left(u\frac{\partial\phi}{\partial y}-\frac{1}{\Lambda^2}v\frac{\partial\phi}{\partial x}\right)\frac{\partial\phi}{\partial y}, \tag{B1}$$

$$\frac{\partial v}{\partial t}+\frac{1}{N}\left(u\frac{\partial v}{\partial x}+v\frac{\partial v}{\partial y}\right)$$
$$=-\Lambda^2\frac{\partial p}{\partial y}+\frac{1}{H_a^2}\left(\frac{1}{\Lambda^2}\frac{\partial^2 v}{\partial x^2}+\frac{\partial^2 v}{\partial y^2}\right)$$
$$+2\left(u\frac{\partial\phi}{\partial y}-\frac{1}{\Lambda^2}v\frac{\partial\phi}{\partial x}\right)\frac{\partial\phi}{\partial x}, \tag{B2}$$

$$\frac{\partial^2 p}{\partial x^2}+\Lambda^2\frac{\partial^2 p}{\partial y^2}$$
$$=-\frac{1}{N}\frac{\partial}{\partial x}\left(u\frac{\partial u}{\partial x}+v\frac{\partial u}{\partial y}\right)-\frac{1}{N}\frac{\partial}{\partial y}\left(u\frac{\partial v}{\partial x}+v\frac{\partial v}{\partial y}\right)$$
$$+\frac{\partial}{\partial x}\left[-2\left(u\frac{\partial\phi}{\partial y}-\frac{1}{\Lambda^2}v\frac{\partial\phi}{\partial x}\right)\frac{\partial\phi}{\partial y}\right]$$
$$+\frac{\partial}{\partial y}\left[2\left(u\frac{\partial\phi}{\partial y}-\frac{1}{\Lambda^2}v\frac{\partial\phi}{\partial x}\right)\frac{\partial\phi}{\partial x}\right]$$
$$+\frac{1}{H_a^2}\left(\frac{1}{\Lambda^2}\frac{\partial^2 D}{\partial x^2}+\frac{\partial^2 D}{\partial y^2}\right)+\frac{D}{\Delta t}, \tag{B3}$$

where

$$D\equiv\frac{\partial u}{\partial x}+\frac{\partial v}{\partial y}. \tag{B4}$$

Although D is identically zero due to the continuity equation, it is retained as a correction term in order to prevent the accumulation of numerical errors.

If we take $\Lambda\to\infty$ in the above equations, Eqs. (B2) and (B3) reduce to $\partial p/\partial y=0$ and $\partial^2 p/\partial y^2=0$, respectively, and then it becomes impossible to solve the problem.

In order to avoid this difficulty, we integrate Eq. (B3) from $y=0$ to $y=1$. Considering the boundary condition Eq. (31), we have

$$\frac{\partial^2}{\partial x^2}\int_0^1 p\,dy$$
$$=-\frac{1}{N}\frac{\partial}{\partial x}\int_0^1\left(u\frac{\partial u}{\partial x}+v\frac{\partial u}{\partial y}\right)dy$$
$$+\frac{1}{H_a^2}\left(\frac{\partial^2 u}{\partial x\,\partial y}\right)_{y=1}$$
$$+\frac{\partial}{\partial x}\int_0^1\left[-2\left(u\frac{\partial\phi}{\partial y}-\frac{1}{\Lambda^2}v\frac{\partial\phi}{\partial x}\right)\frac{\partial\phi}{\partial y}\right]dy$$
$$+\frac{1}{H_a^2\Lambda^2}\frac{\partial^3\Psi_w}{\partial x^3}+\frac{1}{\Delta t}\frac{\partial\Psi_w}{\partial x}, \tag{B5}$$

where $\Psi_w=\int_0^1 u\,dy$. And then, taking $\Lambda\to\infty$ and $\phi=y\sin x$, Eqs. (B1) and (B5) reduce to Eqs. (30) and (29), respectively.

Since Eq. (B2) reduces to $\partial p/\partial y=0$ for $\Lambda\to\infty$, we have lost the relation which decides v. In this case, we can introduce an assumption as

$$\frac{\partial D}{\partial y}=0. \tag{B6}$$

By integrating Eq. (B4) with y under this assumption, we have

$$D=\frac{\partial\Psi_w}{\partial x} \tag{B7}$$

and Eq. (28).

APPENDIX C: STABILITY OF THE FLOW FOR SMALL N

In the case of small N and large H_a, Reynolds number is so large that the assumption of laminar flow in Sec. III C might be uncertain, though it is known that the existence of the magnetic field stabilizes the flow in general.

On considering the linear stability problem for $N\ll 1$, $H_a\gg 1$, and $K\ll 1$, we may notice the following three factors for this problem: (i) The undisturbed flow has exponential boundary layers; (ii) the undisturbed flow is not strictly a parallel flow; and (iii) the disturbances are directly affected by the magnetic field.

The boundary layer on a flat plate with constant suction has similar factors to (i) and (ii). However, according to the analysis of Hughes and Reid,[13] the effect of (ii) is not dominant for the stability of the flow. On the other hand, Hartmann flow under a uniform transverse magnetic field has the same factors as (i) and (iii). But, according to the analysis of Lock,[14] the effect of (iii) is not essential for that flow. The dominating factor for stabilizing the flow field is (i) in both problems.

If the effect of the factors (ii) and (iii) is neglected on the analogy of the results of Hughes and Reid and Lock, the critical Reynolds number may be a value as large as that in their cases. Then we suppose

$$R_c\sim 50\,000, \tag{C1}$$

where $R=\rho_L U_0\delta/\eta_L$ is the Reynolds number based on the thickness δ of the boundary layer. In the present problem, since $\delta=h/H_a$, laminar flow may be possible for

$$N>H_a\Lambda/50\,000. \tag{C2}$$

In Sec. III, we have assumed $\Lambda\to\infty$ in order to simplify the problem. We do not know the minimum Λ for which the analysis in Sec. III C is still valid, but we anticipate the laminar flow can be realized if the condition (C2) is satisfied.

[1] R. N. Sudan, J. Appl. Phys. 34, 641 (1963).
[2] T. C. Wang and S. J. Dudzinsky, AIAA J. 5, 107 (1967).
[3] D. J. Cerini and D. G. Elliott, AIAA J. 6, 503 (1968).
[4] K. Ueno, R. Ishii, and S. Morioka, Fluid Dyn. Res. 6, 53 (1990).
[5] M. Garnier, Prog. Astronaut. Aeronaut. 100, 589 (1985).
[6] J. Hartmann, Det. Kgl. Dan. Videns. Selsk. Math. Fys. Medd. 15, 1 (1937).
[7] G. W. Sutton and A. Sherman, *Engineering Magnetohydrodynamics* (McGraw-Hill, New York, 1965).
[8] J. C. R. Hunt and K. Stewartson, J. Fluid Mech. 23, 563 (1965).
[9] F. H. Harlow and J. E. Welch, Phys. Fluids 8, 2182 (1965).
[10] T. Kawamura and K. Kuwahara, AIAA Paper No. 84-0340, 1984.
[11] G. K. Batchelor, *An Introduction to Fluid Dynamics* (Cambridge U. P., Cambridge, 1967).
[12] A. H. Nayfeh, *Perturbation Methods* (Wiley, New York, 1973).
[13] T. H. Hughes and W. H. Reid, J. Fluid Mech. 23, 715 (1965).
[14] R. C. Lock, Proc. Roy. Soc. London Ser. A 233, 105 (1955).